Desalination and Water Treatment
www.deswater.com
doi: 10.5004/dwt.2022.27960

245 (2022) 129–143
January

Synthesis of 6-cellulose-triethylenetetramine-glutaraldehyde for removal of toxic chromium from an aquatic environment

Ahmed El Nemr*, Ahmed Eleryan, Safaa Ragab

Environmental Division, National Institute of Oceanography and Fisheries, NIOF, Kayet Bey, Elanfoushy, Alexandria, Egypt, email: ahmedmoustafaelnemr@yahoo.com/ahmed.m.elnemr@gmail.com (A. El Nemr), aeleryan71@yahoo.com (A. Eleryan), Safaa_ragab65@yahoo.com (S. Ragab)

Received 13 May 2021; Accepted 31 October 2021

ABSTRACT

Cellulose linked with triethylenetetramine glutaraldehyde (CTG) compound was prepared from the dissolved rice husk cellulose in ionic liquid (dimethylacetamide DMAA/LiCl) by treating with *p*-toluenesulphonyl chloride followed by a substitution reaction with triethylenetetramine (TETA) in the presence of sodium iodide and then condensed with glutaraldehyde. The prepared CTG sample was characterized by FTIR, SEM and EDX analysis. The CTG was evaluated as a valuable material for the adsorption of toxic chromium from an aquatic environment. The maximum adsorption capacity of toxic chromium was achieved at an acidic pH value (1.5). The Freundlich isotherm model fitted to the experimental data slightly better than the Langmuir isotherm model, but both models are highly better than Temkin isotherm model, which proposes that the adsorption mechanism is heterogeneous adsorption. The maximum adsorption capacity of Cr(VI) ions by CTG is 188.68 mg/g, as obtained from the Langmuir model. The adsorption process was found to follow the kinetic model of pseudo-second-order with a rate constant ranging from 1.343 to 50.795 g/mg min. The mass transfer was also studied using an intraparticle diffusion model, which revealed that as the initial Cr(VI) ions concentration increased, the diffusion fraction within the particles increased.

Keywords: Triethylenetetramine; Glutaraldehyde; Rice husk cellulose; Hexavalent chromium; Adsorption

1. Introduction

It is an excellent purpose to develop different kinds of adsorbent from highly available, low-cost, and naturally biodegradable materials such as agriculture residue like sugar bagasse, corn straw, rice straw, and rice husk [1,2]. It causes a big problem known as "black clouds" due to the intensive burning of these wastes, representing a severe economic loss [3]. These wastes can be transformed to economy added value by converting them to activated carbon and modified cellulose materials with many useful applications [4–10]. The physicochemical and thermal properties of cellulose are affected by its isolation techniques such as using acid hydrolysis or chemical swelling in ionic liquids [11,12], electron beam irradiation [13], steam explosion treatment [14,15], the alkaline pulping process by sodium hydroxide [16] and enzyme-assisted isolation [17,18].

One of the essential applications of cellulose derivatives is the removal of pollutants from aquatic environments and industrial wastewater [19–22]. Cellulose submitted too many types of modifications before using for pollutants removal to improve its adsorption efficiency, physicochemical properties, and mechanical properties [23,24]. The bio-sorbent capacity of modified cellulose can be improved by specific extra functionalization with *N*-rich functional groups to increase its chelating ability [25,26].

Many toxic effluents of hazardous chemicals are expelled every day into aquatic environments; oceans, seas,

* Corresponding author.

rivers, and lakes worldwide [27–36]. To overcome the water deficiency problems in the future, recycling contaminated waters becomes one of the essential methods to make it suitable for reuse [37,38]. Great efforts were made to treat wastewaters from different industrial processes, agriculture, energetic plants, and domestic uses, especially those containing toxic heavy metal ions [39–48]. Facile preparation of amine-rich polyamidoamine gel for Cr(VI) ions removal with high efficiency [49]. Functionalization of natural peach gum polysaccharide with multiple amine groups to remove toxic Cr(VI) ions from water has been reported [50].

Environmental contamination with various heavy metals such as copper, cadmium, mercury, chromium, nickel, lead and zinc commonly has pollution and toxicity problems to the humans, animals, water, sediment, and air [47]. Pollution with heavy metals is a significant environmental problem because heavy metals accumulate throughout the food chain and have high toxic effects on the environment [48].

Hexavalent chromium [Cr(VI)] has environmentally threats, and its removal from water has significant importance for human beings health [51,52]. According to World Health Organization (WHO) guidelines, the safe permissible limit Cr(VI) ions concentration in drinking water is 0.05 mg/L [53]. The sources that contaminate water with Cr(VI) ions are mainly industrial processes such as pigment, electroplating, leather processing, metal cleaning and mining [5,54]. Many physical and chemical processes have been used to remove and detoxify hexavalent chromium from water. The adsorption method has many advantages, by using inexpensive absorbents, low operating costs, clean operating, and economically feasible to remove pollutants from contaminated solution [55]. Cellulose as carbohydrate polymers is a more suitable starting material to make a biocompatible, biodegradable, promising adsorbent, low-cost and highly available adsorbent [56].

This paper concern with isolation of cellulose from rice husk and convert it to an effective modified cellulose by a good leaving group as tosyl group via reaction with *p*-toluenesulfonyl chloride (TSCl) in presence of triethylenamine (TEA) as an organic base, then functionalization of 6-tosylated cellulose with TETA followed by extra functionalization with glutaraldehyde. The final product, 6-cellulose-TETA-glutaraldehyde (CTG), was tested to adsorb toxic chromium ions from its water solutions. The synthesized CTG shows a comparable adsorption behavior to the previously reported adsorbent materials.

2. Materials and methods

2.1. Materials and instrument

Sodium hydroxide scales, sodium hypochlorite, acetic acid, hydrogen peroxide was purchased from ElNasr Pharmacuitical Chemicals Co., Egypt. Dimethylacetamide (DMAA), triethylamine (TEA), *p*-toluenesulfonyl chloride (TSCl), ethanol, triethylenetetramine (TETA), dimethylsulfoxide (DMSO), dimethylformamide (DMF), glutaraldehyde, acetonitrile, and potassium dichromate were supplied by Sigma Aldrich, and was used without further purification. Bruker VERTEX 70 spectrometer coupled to platinum ATR unit instrument has been used for FTIR analysis in the range of 4,000–400 cm^{-1}. The UV-visible double beam spectrophotometer (SPEKOL 1300-ANALYTIK JENA AG-Germany) was used to analyse Cr(VI) ions concentration.

2.2. Isolation of rice husk cellulose

Cellulose was obtained from rice husk as stated nearly by cooking treatments for removing lignin and hemicellulose followed by bleaching process in two steps to increase the cellulose content [9,11,12]. A dried rice husk (500 g) in a round bottom flask (5 L) and 2% NaOH solution (4 L) was heated in a water bath for 2 h at 70°C for two times with new 2% NaOH solution (4 L). The reaction mixture was filtered and washed with tap water to eliminate the black lacquer. The resulting pulp was subjected to two steps of bleaching; first, the pulp was treated with 8% sodium hypochlorite (NaOCl) (4 L) at 70°C for 2 h, followed by the second step as extra bleaching by 5% hydrogen peroxide H_2O_2 (4 L) at 70°C for 2 h. The mixture was filtered off, repeatedly washed with tap water followed by distilled water, and the resulting white pulp was oven-dried at 50°C and powdered to be ready for the next step.

2.3. Chemical modification of rice husk cellulose

2.3.1. Preparation of tosylated rice husk cellulose

In a round bottom flask (1 L), 10 g of rice husk cellulose was heated in 240 mL of DMAA solvent at 130°C. Then 20 g lithium chloride was added to the reaction mixture with stirring at 100°C, and stirring was continued to have a bright-yellow viscous solution and complete dissolution of cellulose [47,57–59]. Then, reaction mixture was cooled in an ice/water bath followed by adding a mixture of TEA (77 mL) and DMAA (50 mL) drop wise with stirring at 8°C, then add drop by drop a solution of *p*-toluenesulfonyl chloride (52 g) in 110 mL of DMAA solvent within 1 h with stirring. Complete the reaction for 24 h at 10°C. After that, the flask was kept in the refrigerator overnight. The darkling of the solution is an indication of complete reaction. The reaction mixture was poured into 2.5 L ice-cold water. Then, filtered, washed with 5 L water followed by 0.5 L ethanol, and dried at 50°C in an oven.

2.3.2. Functionalization of tosylated rice husk cellulose with TETA

Add a mixture of TETA (23 mL) and DMF (100 mL) to 10 g of tosylated rice husk cellulose and KI (8 g), and the mixture was heated for 36 h at 60°C under stirring. The mixture is poured into ice-water and filtered to give a dark brown gummy material [47,57–59].

2.3.3. Extra functionalization of Cell-TETA by glutaraldehyde

10 g of the above dark brown gummy substance was dissolved in 10 mL ethanol, then 20 mL glutraldehyde was added, and the reaction mixture was stirred for 24 h at 100°C. The reaction mixture was cooled, filtered, washed with distilled water, and then dried at 50°C [47,60]. The total reaction is shown in Fig. 1.

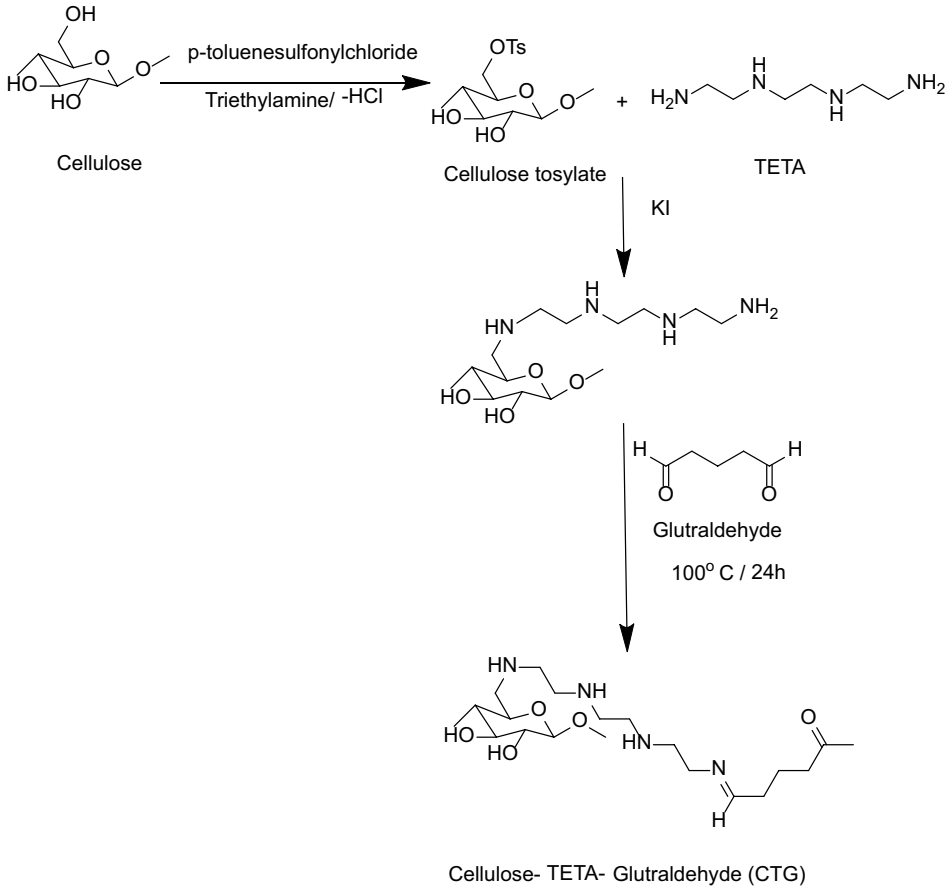

Fig. 1. Functionalization of cellulose to prepare cellulose-TETA-glutraldehyde (CTG).

2.4. Adsorption batch experiments

2.4.1. Preparation of Cr(VI) solution

By dissolving 2.828 g of potassium dichromate in 100 mL double distilled water and then completing the volume to 1 L with double distilled water, a 1,000 mg/L stock solution of Cr(VI) ions was prepared. Dilution of the stock solution to the concentrations needed for standard and batch experimental solutions yielded various Cr(VI) ions solutions. 0.1 M HCl and NaOH solutions were used to change the pH at the start and during the experiment to the appropriate values. The concentration of Cr(VI) was determined by a UV-visible spectrophotometric method based on a complixation reaction (red-violet colored complex) with 1,5-Diphenylcarbazide (G.R., E. Merck) [9]. The concentration of the formed complex with red-violet color was analyzed using spectrophotometer at a wavelength, λ_{max} of 540 nm.

2.4.2. Effect of pH on Cr(VI) ions adsorption

Using 50 mg/L chromium ions and 2.0 g/L CTG at different pH values (1.0–10.5), the effect of pH on the equilibrium adsorption of Cr(VI) ions was investigated. At room temperature (25°C ± 2.0°C), the samples were shaken at a speed of 200 rpm. After determining the remaining chromium ion concentration and calculating the elimination percentage, the minimum contact time needed to achieve equilibrium was 120 min [6].

2.4.3. Effect of CTG dose, isotherm and kinetics studies

The impact of CTG adsorbent dose on the chromium ions equilibrium uptake was measured by shaking different weights of CTG (0.05–0.25 g) and 100 mL of various Cr(VI) ions concentrations (25–150 mg/L) separately, implying that every Cr(VI) ions concentration was measured by shaking with all the above weights of CTG to the equilibrium uptake. The concentration of Cr(VI) ions in the reaction mixture was measured at different contact times, and the percentage of removal with time was calculated. After shaking the flasks for 120 minutes, the reaction mixture was analysed to determine the residual chromium concentration at equilibrium; only the mean values were recorded after all trials were replicated, and the overall observed deviation was less than 5% [6].

3. Results and discussion

3.1. Adsorbent characterization

3.1.1. FTIR spectra of modified cellulose

Fig. 2 shows the FTIR spectra of rice husk cellulose, the result of each stage of modification, as well as unloaded and

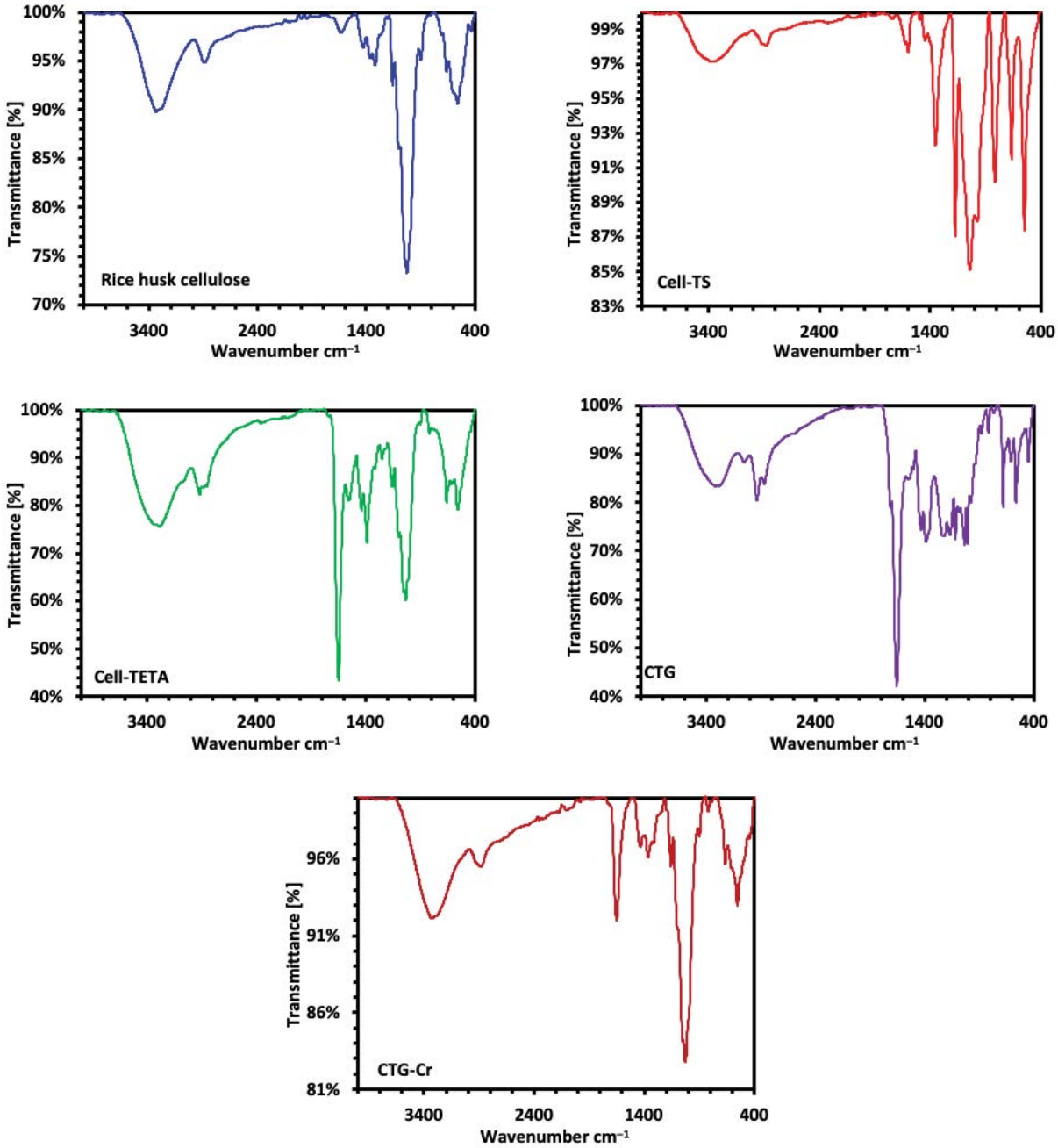

Fig. 2. FTIR of rice husk cellulose, Cell-TS, Cell-TETA, CTG, and CTG-Cr compounds.

loaded modified cellulose with Cr(VI) ions. The OH groups in rice husk cellulose have a band at 3,331 cm^{-1}, the CH_2OH has a band at 2,889 cm^{-1}, and the C–O–C of the glucose ring in cellulose has bands at 898, 1,025 and 1,157 cm^{-1}. The first product, cellulose tosylate, has three bands at 1,353, 1,173 and 816 cm^{-1} due to the OH groups, 2,883 cm^{-1} due to the CH_2OH, and bands at 1,043, 973 cm^{-1} due to the C–O–C. The tosyl group is defined by three bands at 1,353, 1,173 and 816 cm^{-1} [24,61,62].

The bands at 3,268 cm^{-1} in the FTIR of Cell-TETA could be attributed to OH groups, while the bands at 2,938 and 2,877 cm^{-1} could be attributed to the C–H (CH_3, CH_2) bond elongation, which is typical of materials with saturated carbons or sp^3. The C=N bond is represented by the band at 1,650 cm^{-1} stretching frequency. The C–O–H bond bending is responsible for the band at 1,425 cm^{-1}; this band is also overlooked for the CH_2 bands [63]. The peak at 1,528, 1,440, 1,390 and 1,310 cm^{-1} are due to the NH groups. The FTIR analysis of CTG shows peak at 3,316 cm^{-1} for OH, 3,055 cm^{-1} for NH groups and peaks at 2,937 and 2868 cm^{-1} are due to the CH_2 groups. A new peak at 1713 cm^{-1} is related to CHO group, and the peak at 1,656 cm^{-1} is corresponding to C=N and C=O groups. FTIR analysis of CTG-Cr shows changes in the positions of the peaks. The peak at 3,336 cm^{-1} for OH

groups, the peaks of NH many shifted and disappeared due to the complex formation with the Cr. The peak at 1,713 cm^{-1} due to CHO disappeared due to the complex formation with Cr(VI). As well as the peak intensity at 1,651 cm^{-1} decreased due to the complex formation. The asymmetric stretching vibrations of the C–O–C group have a peak at 1,021 cm^{-1}. Since hexavalent chromium is a strong oxidising agent, it oxidises and is reduced to Cr(III). The existence of Cr is confirmed by the adsorbent's green color after loading Cr(III). Maxcy et al. [64] proposed a similar method for the adsorption of Cr(VI) by thiourea.

3.1.2. SEM and EDX analyses

The morphology of the CTG surface before and after the Cr(VI) ions adsorption process was studied using scanning electron microscopy (SEM) (Fig. 3). The images in Fig. 3 show that the surface morphology changes after adsorption of chromium ions because the pores in Fig. 3a were fully filled with chromium ions, as seen in Fig. 3b.

Fig. 4a shows the EDX plot of CTG samples before and after the Cr(VI) ions removal process, respectively. Fig. 4b further proved the presence of chromium ions on the CTG samples surface. The presence of chlorine on the surface of CTG sample after Cr(VI) ions adsorption may be attributed to the pH adjustment using HCl. The EDX analysis showed 12.30% of the nitrogen that confirmed the chemical modification of cellulose with TETA (Table 1).

3.2. Kinetic studies

The following measures may be used to deduce the Cr(VI) adsorption mechanism: (i) Electrostatic driving forces caused negatively charged chromium species (e.g., $HCrO^{4-}$) to migrate to positively charged adsorbent surface sites (e.g., quaternary amine groups). (ii) At acidic conditions, Cr(VI) is reduced to Cr(III) on the surface of the adsorbent by neighboring electron-donor groups. The formed Cr(III) ions can then bind to anionic groups (such as carboxyl and hydroxyl groups) and make complexes with the amine and aldehyde groups on the adsorbent surface.

3.2.1. Effect of pH on Cr(VI) ions uptake

Most contaminants are removed by adsorption, and the pH parameter is the most important factor in this process. At different pH values (1.0–10.5), the optimum pH value for Cr(VI) ions adsorption by CTG was investigated. Fig. 5 shows the relationship between Cr(VI) ions removal and pH values. This demonstrates that the lowest uptake value was observed at pH 8.4 and the highest percentage of removal occurred at pH 1.0, and that it decreased dramatically as the pH value increased. However, no further removal occurred at pH < 1. Changes in the pH of the solution may affect the protonation degree of the hydroxyl and amine groups linked with the surface charge of the CTG adsorbent.

On the other hand, changes in the pH of a solution can affect the forms of Cr(VI) ions in water [49, 50]. In solution, the most dominant Cr(VI) ions species are $HCrO_4^-$, $Cr_2O_7^{2-}$, $Cr_4O_{13}^{2-}$ and $Cr_3O_{10}^{2-}$, which might be found at optimum sorption pH 1.0 and adsorbed mainly by electrostatically nature and complex formation with CHO, C=N and NH. Hydronium ions surround the adsorbent surface to form a positive charged CTG surface ($CTG\text{-}H^+$) at very low pH values, increasing the attractive forces between Cr(VI) ions and $CTG\text{-}H^+$ binding sites. The overall surface charge on CTG became negative as the pH increased, reducing the adsorption of negative charged Cr(VI) ions. It is also recognized that when there are a high concentration of Cr(VI) ions, the $Cr_2O_7^{2-}$ ions precipitate at higher pH values [65]. It's

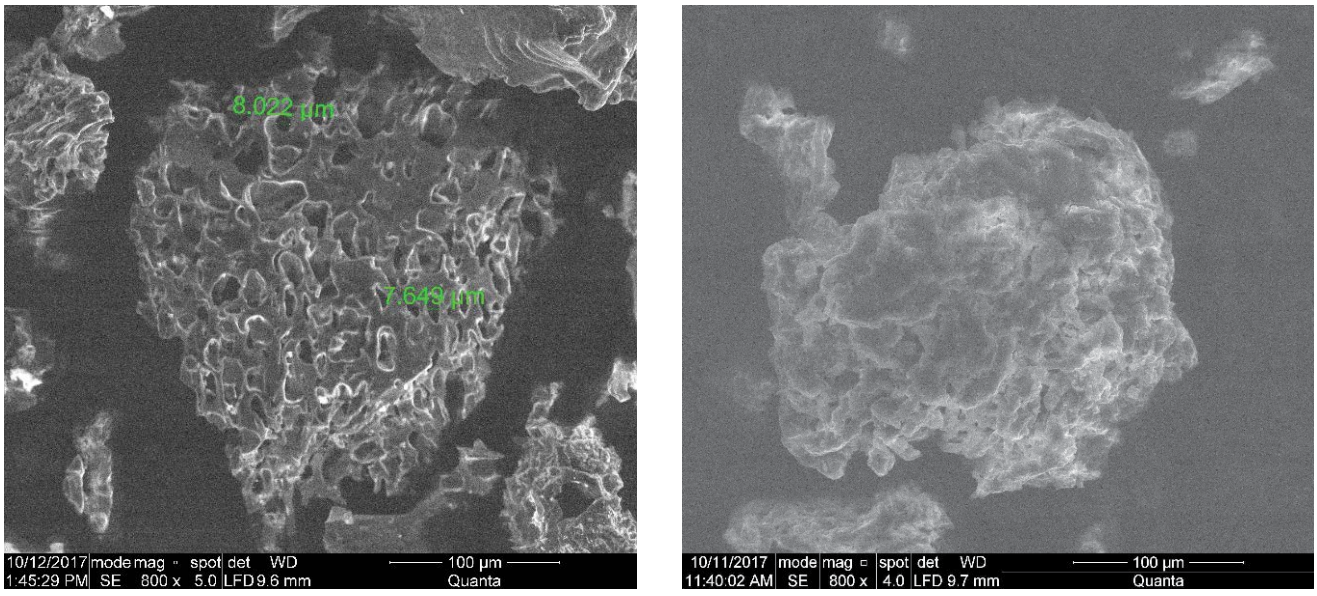

(a) (b)

Fig. 3. (a) SEM of CTG before Cr(VI) ions adsorption and (b) SEM of CTG after Cr(VI) ions adsorption.

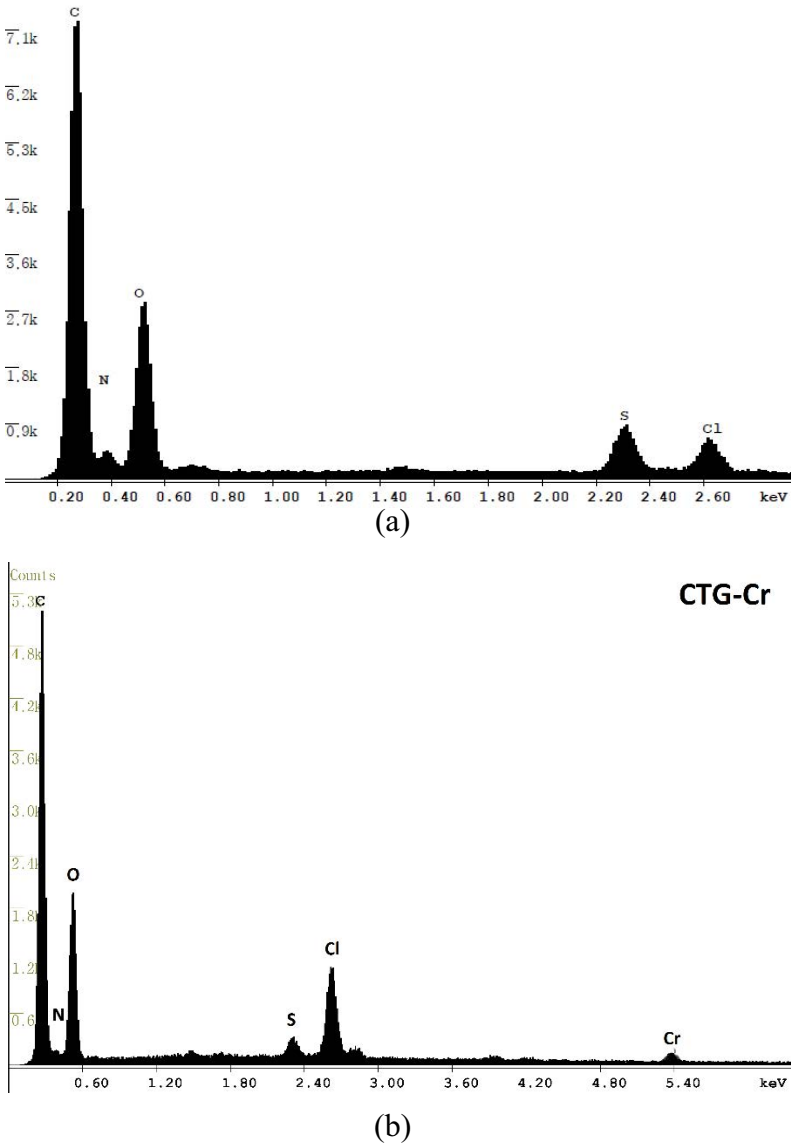

Fig. 4. (a) EDX plot of CTG before Cr(VI) ions adsorption and (b) EDX plot of CTG after Cr(VI) ions adsorption.

worth noting that chromium's composition and valiancy are pH-dependent, so the adsorption mechanism is also affected by its form.

3.2.2. Initial Cr(VI) ions concentration and contact time effects

The high initial concentration of Cr(VI) ions increased the biological absorption rate due to the high concentration, as it plays an important role in overcoming the mass transfer resistance of the metal ions between the aqueous and solid stages. Fig. 6a shows the percentage removal of Cr(VI) at pH 1.0 as a function of rising contact time using CTG. With increasing time and CTG concentrations, the percentage of Cr(VI) ions removed increased. The adsorption rate of Cr(VI) ions onto CTG was found to be sluggish after 65% of Cr(VI) ions were adsorbed in the time range of 5–20 min. This was possibly caused by repulsion between the negatively adsorbed Cr(VI) ions on the surface of the CTG and the available Cr(VI) anionic ions in the solution or electrostatic barrier, as well as the slow pore diffusion of Cr(VI) ions in the bulk of the CTG. Because of the presence of a strongly acidic solution (pH 1.0), electrostatic reactions would have the most significant on the adsorption. Adsorption is regulated by the attraction and repulsion between the charged surface of CTG and the negative chromium ions.

Using different doses of CTG, Fig. 6b shows the relationship between quantities of Cr(VI) ions adsorbed at equilibrium (q_e) and their initial concentration. When the maximum Cr(VI) ions adsorption onto CTG was extended, the equilibrium was found to be nearly 120 min. In addition, in Fig. 6a and b, the effect of initial Cr(VI) ions concentration on adsorption ability into CTG is shown, with percentage removal of Cr(VI) ions estimated at 120 min of contact time for five different initial chromium concentrations. The percentage of removed Cr(VI) ions decreased as

Table 1
Results of EDX analysis of CTG prior and after chromium ions adsorption process

Elements	CTG before adsorption %	CTG after adsorption %
Carbon	54.38	53.31
Oxygen	29.26	21.29
Nitrogen	12.3	11.22
Sulfur	2.24	2.08
Chlorine	1.82	8.96
Chromium	0.00	3.14

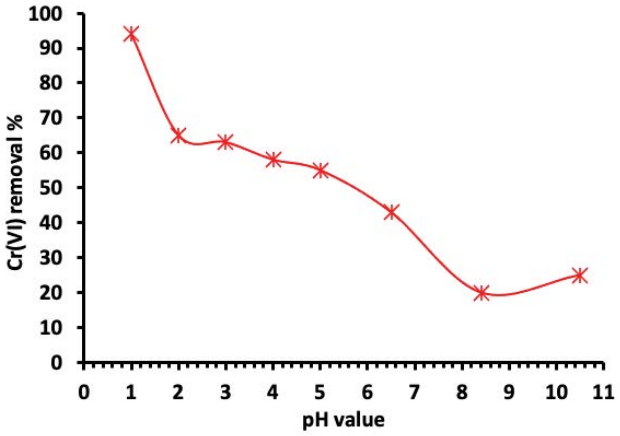

Fig. 5. pH effect investigation on chromium ions (75 mg/L) adsorption onto CTG (2.50 g/L) at 25°C ± 2°C.

the initial concentration of Cr(VI) ions increased, implying that electrostatic interactions mediate the adsorption mechanism.

3.2.3. Adsorption of metals as a feature of adsorbent dose

The effect of CTG dosage on the adsorption of Cr(VI) ions from aqueous solutions was investigated using five different adsorbent concentrations and five different initial chromium concentrations. CTG's specific surface area, which can be defined as the portion of the total area available for Cr(VI) ions adsorption, is proportional to the amount of Cr(VI) ions adsorbed. CTG concentrations ranged from 0.5 to 2.5 g/L at pH 1.0, with initial chromium concentrations ranging from 25 to 150 mg/L. For a given initial Cr(VI) ions concentration, the equilibrium concentration (C_e) of Cr(VI) ions decreases as CTG concentration increases, as shown in Fig. 6c. This is because higher adsorbent doses result in more adsorbent surface area and pore volume usable for adsorption.

3.2.4. Isotherm data analysis

Isotherm analysis is critical for determining an equation that correctly reflects adsorption results and can design adsorption columns. Adsorption isotherms may also be used to explain how a solute interacts with adsorbents, which helps optimize adsorbent usage. For dissolved structures, the Langmuir and Freundlich models are the most commonly known surface absorption models. Langmuir, Freundlich, and Temkin isotherm models were used to analyze the results. The most suitable isotherm was determined by linear regression, and the parameters of the isotherms were calculated using the intercept and linear slope of the various isotherm models.

The maximum adsorption capacity conforming to complete monolayer coverage on the CTG was calculated using the Langmuir isotherm model since the saturated monolayer isotherm can be defined by the non-linear equation of Langmuir Eq. (1) [6,66].

$$q_e = \frac{Q_m K_L C_e}{1 + K_L C_e} \tag{1}$$

where C_e represents the equilibrium concentration (mg/L), q_e represents the sum of metal ion adsorbed (mg/g), Q_m represents a full monolayer (mg/g), and K_L represents an adsorption equilibrium constant (L/mg) that is related to the apparent energy of adsorption. Eq. (1) can be transformed into Eq. (2) by linearizing it [67,68]. The most general linear form of the Langmuir model is Eq. (2), and the results for the adsorption of Cr(VI) onto CTG obtained from this form of the Langmuir model are shown in Fig. 7a and Table 2.

$$\frac{C_e}{q_e} = \frac{1}{K_L Q_m} + \frac{1}{Q_m} \times C_e \tag{2}$$

The chromium ion adsorption onto CTG did not obey the Langmuir isotherm model, according to the results in Table 2. The low correlation coefficients values for all initial chromium concentrations tested demonstrated the Langmuir isotherm models' less applicability to the adsorption of Cr(VI) ions onto CTG (Table 2). The experimental q_e of Cr(VI) ions adsorption on different doses of CTG (0.5–2.5 g/L) is compared to the measured Langmuir equilibrium isotherms q_e obtained from Langmuir model data in Table 3. Since the predicted q_e values agree with the experimental q_e values, the Langmuir isotherm model can be applied to the adsorption of Cr(VI) ions onto CTG, as shown in Table 3. The maximum monolayer capacity (Q_m) of the Langmuir isotherm was 188.68 mg/g.

Based on adsorption heterogeneous energetic distribution of active sites, the Freundlich model was chosen to estimate the adsorption strength of Cr(VI) ions onto the CTG surface. It can be calculated using the non-linear Eq. (3) and

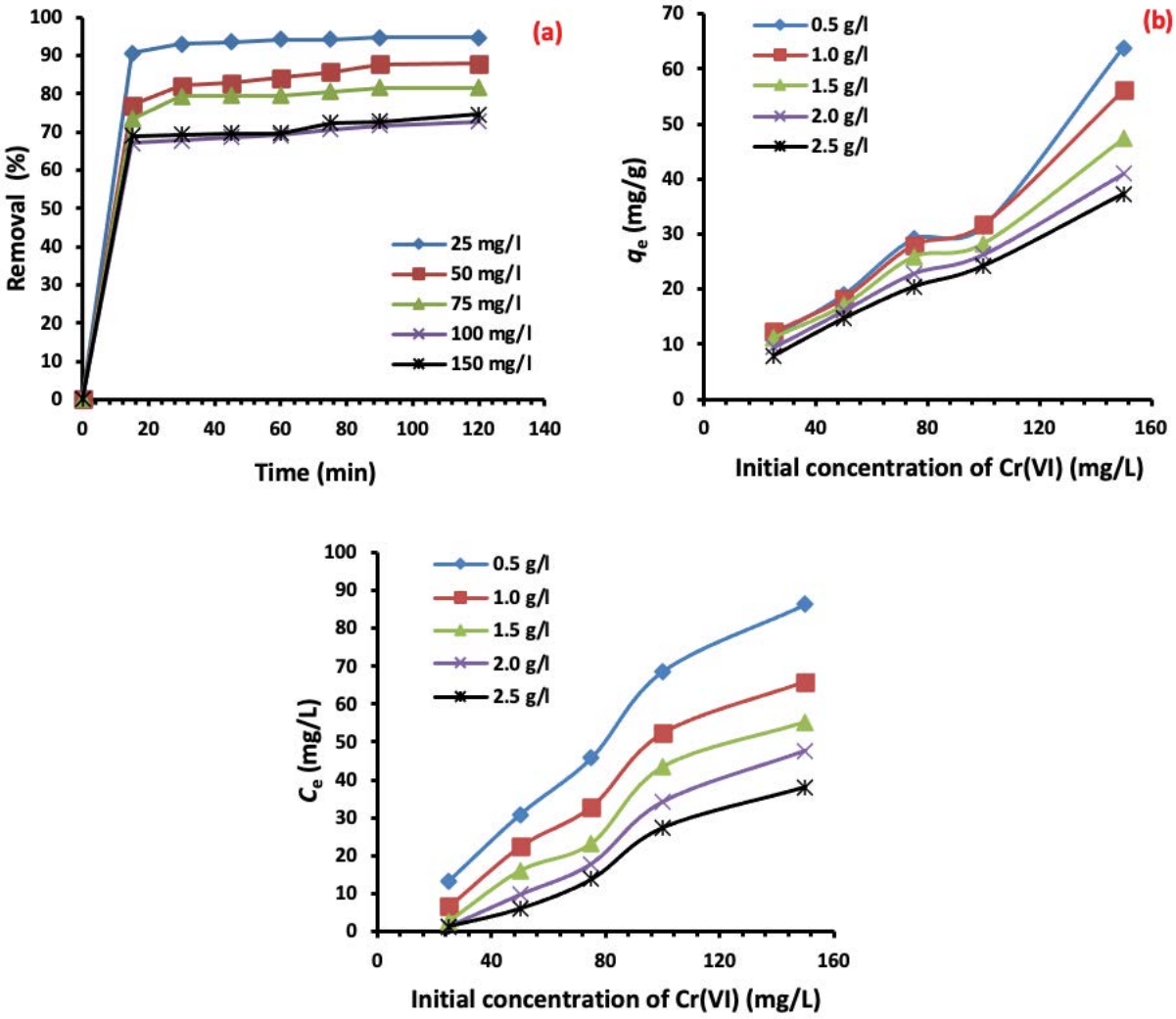

Fig. 6. (a) The impact of contact time on the adsorption of various initial chromium concentrations onto CTG (2.5 g/L) at pH 1.0. (b) The relationship between the initial concentration of Cr(VI) ions and the sum of Cr(VI) ions adsorbed at equilibrium (q_e). (c) The relation between equilibrium concentration (C_e) of Cr(VI) ions and its initial concentration.

assumes a logarithmic decrease in sorption enthalpy as the fraction of occupied sites increases [6,69].

$$q_e = K_F C_e^{1/n} \tag{3}$$

where K_F (mg/g) and n, respectively, represent the adsorption capacity and adsorption intensity of Cr(VI) ions on the CTG. Eq. (3) can be linearized in logarithmic form Eq. (4), and the Freundlich constants can be determined from the linear plot of $\log(q_e)$ against $\log(C_e)$.

$$\log\left(q_e\right) = \log\left(K_F\right) + \frac{1}{n}\log\left(C_e\right) \tag{4}$$

Fig. 7b shows the linear Freundlich isotherm plots for the adsorption of Cr(VI) ions onto CTG. The Freundlich model is somewhat more applicable to CTG than the Langmuir isotherm model, according to the correlation coefficients stated in Tables 2 and 4. The CTG correlation coefficient indicates that the experimental results which match the Freundlich model well. At 25°C, the n values (1.17–2.27) are higher than 1.0, suggesting that CTG preferentially adsorbs Cr(VI) ions. Furthermore, the magnitude of K_F ranged from 20.52 to 22.82, indicating high adsorptive potential and fast Cr(VI) absorption by CTG from an aqueous solution [6,55].

Temkin isotherm model was used to investigate the effects of indirect adsorbent-adsorbent interaction, which stated that due to adsorbent-adsorbent interaction, the adsorption heat of all molecules on the adsorbed surface layer would decrease linearly with coverage. As a result, Temkin adsorption model, which agrees that the fall in adsorption temperature is linear rather than logarithmic, as seen in the Freundlich equation, can be used to calculate the adsorption potentials of the adsorption process. Temkin isothermal method is commonly used in Eq. (5) [70–72].

$$q_e = \frac{RT}{b}\ln\left(A_T C_e\right) \tag{5}$$

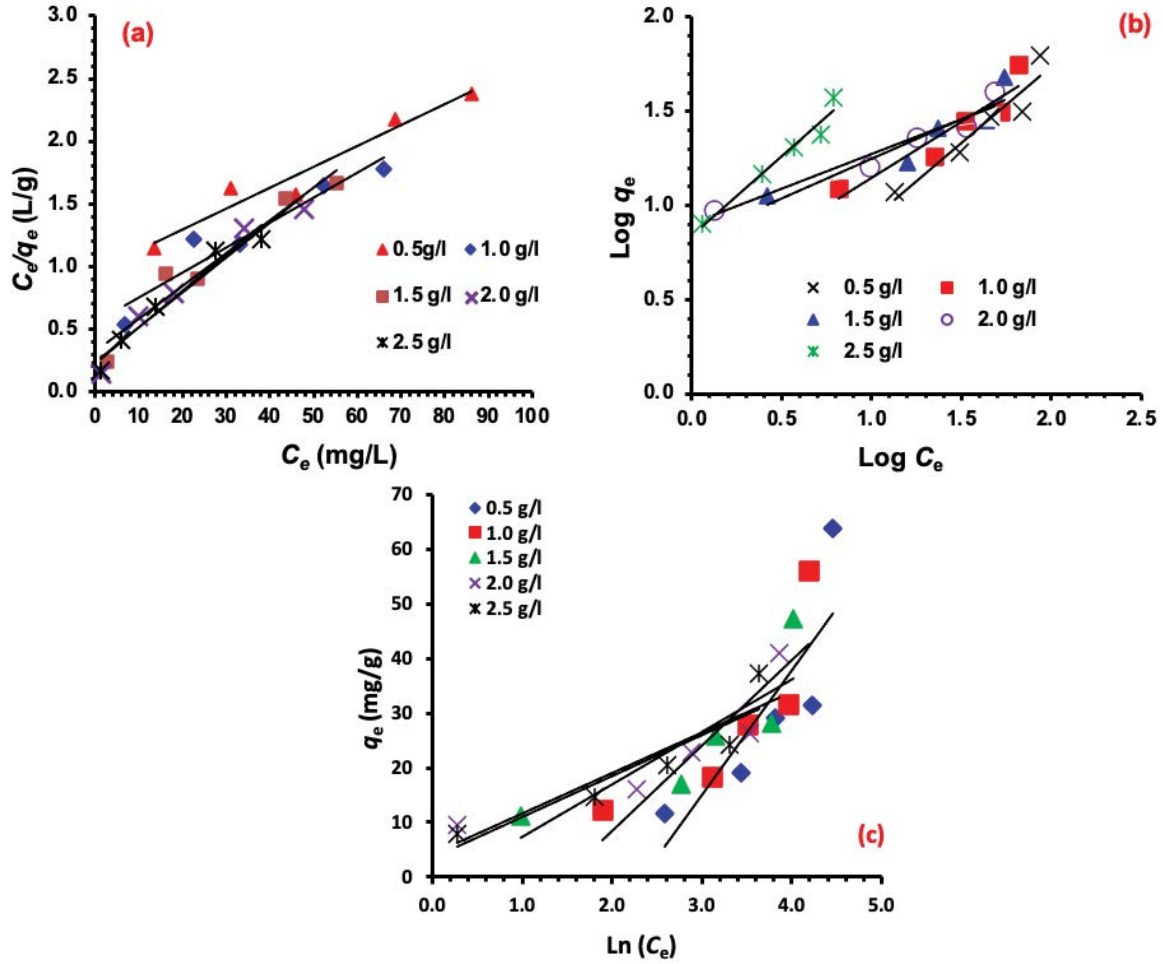

Fig. 7. (a) Langmuir, (b) Freundlich, and (c) Temkin equilibrium isotherm models for the adsorption of Cr(VI) ions (25–150 mg/L) at room temperature (25°C ± 2°C) onto CTG (0.5–2.5 g/L) at pH 1.

The Temkin isotherm Eq. (5) can be derived to the following Eq. (6).

$$q_e = B_T \ln\left(A_T\right) + B_T \ln\left(C_e\right) \tag{6}$$

where $B_T = (RT)/b$ and A_T (L/g) are the constants of Temkin model, which can be measured using a plot of q_e against $\ln(C_e)$. Also, T and R, respectively, are the absolute temperature in Kelvin and the universal gas constant (8.314 J/mol K). The b is a constant related to the heat of adsorption [73,74]. Fig. 7c depicts the Temkin isotherm linear plots for the adsorption results. Because of the low correlation coefficients, the Temkin isotherm cannot be applied to the adsorption of Cr(VI) ions onto CTG (Table 2).

Table 2
Data obtained from the isotherm models analysis of the adsorption of Cr(VI) (25–150 mg/L) onto CTG (0.5 g/L) at room temperature

Isotherm \ CTG (g/L)	Isotherm parameter	0.5 (g/L)
Langmuir	Q_m (mg/g)	188.68
	K_a (L/mg)	0.004
	R^2	0.947
Freundlich	n	1.236
	K_F (mg/g)	1.316
	R^2	0.987
Temkin	A_T (L/g)	0.096
	B_T (mg/L)	22.792
	R^2	0.709

3.2.5. Kinetic and mass transfer investigation

Batch experiments with various chromium concentrations and CTG doses were performed to determine the rate of chromium adsorption by CTG at pH 1.0. To comprehend the dynamics of the adsorption reaction, kinetic adsorption data can be examined. The kinetics of Cr(VI) ions adsorption on CTG are crucial in determining the best-operating conditions for the full-scale batch operation. It's also useful for estimating the adsorption rate and providing crucial information for process design and modelling. The pseudo first-order model is used to investigate the chromium removal mechanism

Table 3
The experimental q_e data of Cr(VI) ions adsorption on different doses of CTG (0. 5–2.5 g/L) were compared to Langmuir equilibrium isotherms (q_e)

CTG (g/L) / Cr(VI) (mg/L)	0.5 g/L		1.0 g/L		1.5 g/L		2.0 g/L		2.5 g/L	
	q_e (exp.)	q_e (cal.)	q_e (exp.)	q_e (cal.)	q_e (exp.)	q_e (cal.)	q_e (exp.)	q_e (cal.)	q_e (exp.)	q_e (cal.)
25	11.63	11.64	12.25	12.19	11.17	11.50	9.47	9.04	7.89	7.58
50	19.08	20.90	18.37	18.57	16.99	16.88	16.12	16.77	14.66	14.87
75	29.18	29.40	28.03	29.49	25.87	26.82	22.86	22.51	20.41	20.13
100	31.43	30.84	31.77	31.93	28.27	27.90	26.33	26.02	24.22	24.42
150	63.78	63.64	56.05	56.85	47.35	47.71	40.94	40.77	37.31	37.90

Table 4
Comparison between Freundlich equilibrium isotherms (q_e) and the experimental q_e data of Cr(VI) ions adsorption on various doses of CTG (0.5–2.5 g/L)

CTG (g/L) / Cr(VI) (mg/L)	0.5		1.0		1.5		2.0		2.5	
	q_e (exp.)	q_e (cal.)	q_e (exp.)	q_e (cal.)	q_e (exp.)	q_e (cal.)	q_e (exp.)	q_e (cal.)	q_e (exp.)	q_e (cal.)
25	11.63	10.73	12.25	10.94	11.17	10.14	9.47	8.87	7.89	8.80
50	19.08	21.15	18.37	22.58	16.99	21.62	16.12	18.56	14.66	15.31
75	29.18	29.07	28.03	28.37	25.87	25.29	22.86	23.29	20.41	22.75
100	31.43	35.29	31.77	33.34	28.27	30.91	26.33	27.64	24.22	25.58
150	63.78	58.50	56.05	52.83	47.35	46.43	40.94	39.54	37.31	38.28

from aqueous medium through CTG [75], pseudo second order [76], intraparticle diffusion [77,78] and Elovich [6,76] kinetic models. Correlation coefficients were used to express the consistency between experimental results and model expected values (R^2 close or equal to 1). When the R^2 value of the Cr(VI) ions adsorption kinetics model is relatively higher, it is more applicable. The kinetic data were analyzed using the pseudo first-order kinetic model [75], which was the first to characterize the adsorption rate in terms of adsorption power. It is generally detailed in equation (7).

$$\frac{dq_t}{dt} = K_1\left(q_e - q_t\right) \tag{7}$$

where q_e and q_t (mg/g), respectively, are the adsorption capacity at equilibrium and at time t. K_1 (min^{-1}) is the rate constant of pseudo-first-order adsorption. Eq. (7) was integrated to linear Eq. (8).

$$\log\left(q_e - q_t\right) = \log\left(q_e\right) - K_1 \times 2.303t \tag{8}$$

Plotting of $\log(q_e - q_t)$ against (t) provides a linear relationship, the K_1 and predicted q_e can be determined, respectively, from the plot slope and intercept (Fig. 8a). The rate differential must be proportional to the strict surface adsorption's first concentration power. The relationship between the initial chromium concentration and the rate of adsorption, on the other hand, will not be linear if pore diffusion is the rate limit of the adsorption process. Even when the R^2 is relatively large, the pseudo-first kinetic model does not suit the experimental data well. The experimental q_e values do not match the measured q_e values obtained from the pseudo-first kinetic model (Table 5) [6]. This demonstrates that a first-order reaction cannot adequately explain the adsorption of Cr(VI) ions onto CTG.

The pseudo second-order model proposed by Ho et al. [76] was used to analyze the adsorption kinetic results, as shown in Eq. (9).

$$\frac{dq_t}{dt} = K_2\left(q_e - q_t\right)^n \tag{9}$$

where K_2 (g/mg min) is known as the adsorption second-order rate constant. Integrating Eq. (9) gave linearized Eq. (10).

$$\frac{t}{q_t} = \frac{1}{K_2 q_e^2} + \frac{1}{q_e}(t) \tag{10}$$

This model was used to calculate the initial adsorption rate (h) by using Eq. (11):

$$h = K_2 q_e^2 \tag{11}$$

If the t/q_t vs. t plot indicates a linear relationship, this model can be used. The intercept and slope of these plots (Fig. 8b) were used to measure K_2 and q_e values, which showed strong agreement between experimental and measured q_e values at various Cr(VI) ions and CTG concentrations with $R^2 \geq 0.999$ (Table 5). The pseudo second-order kinetic model was found to be valid for the adsorption of Cr(VI) ions onto CTG for all Cr(VI) ions and adsorbent concentrations tested. Furthermore, the h values

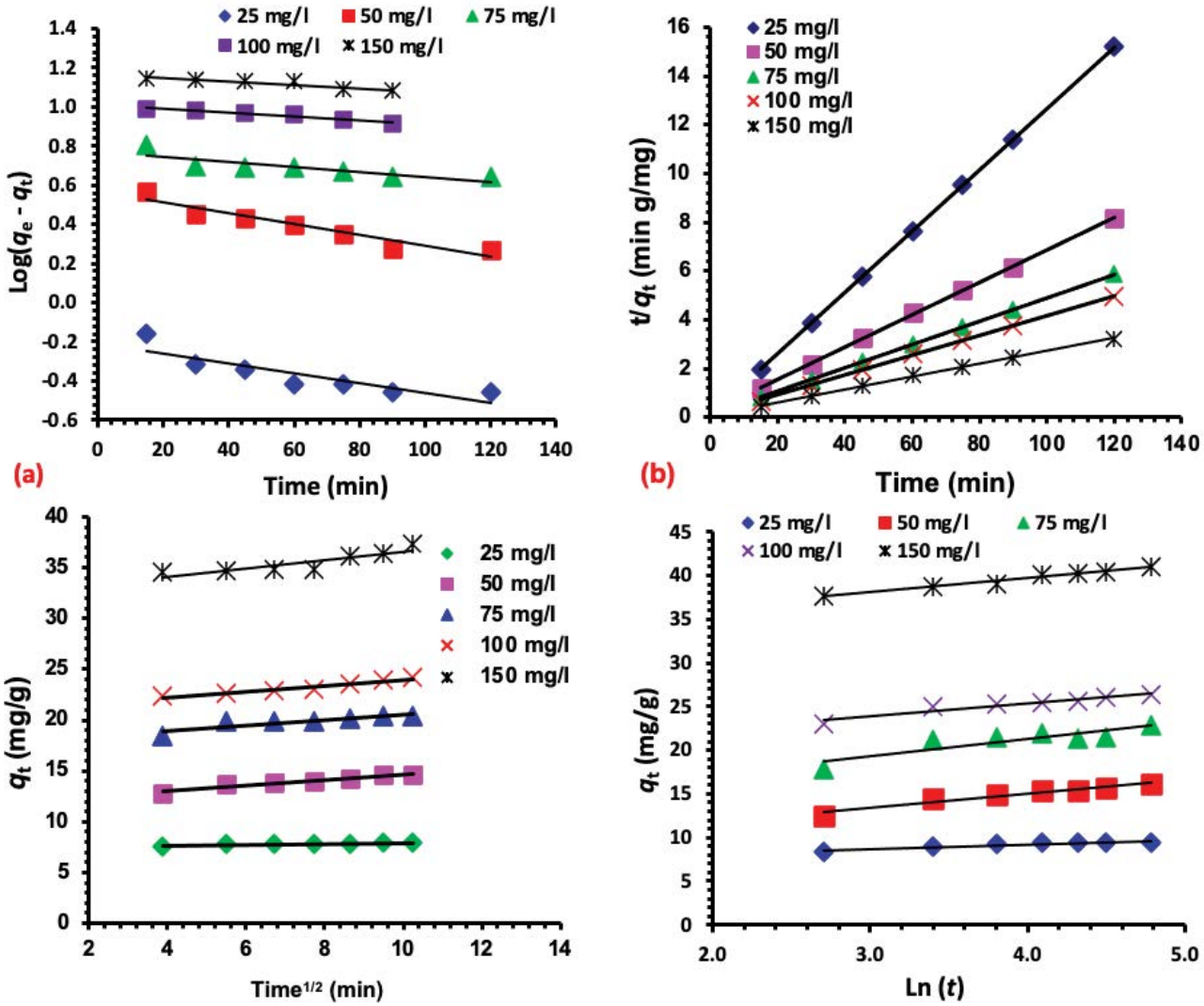

Fig. 8. (a) Pseudo-first-order kinetics, (b) pseudo-second-order kinetics, (c) intraparticle diffusion kinetics, and (d) Elovich kinetics for Cr(VI) ions (25–150 mg/L) adsorption at room temperature (25°C ± 2°C) onto CTG (2.5 g/L) at pH 1.0.

play no part, whereas the K_2 values decrease as the initial Cr(VI) ions concentration rises for all CTG doses.

Solute molecules migrate from the solution medium to the surface of the solid adsorbate, followed by solute molecules diffusing into the interior of its pores, which is expected to be a slow process. Hence, this stage is called a rate-determining step in the multi-phase adsorption process. The intraparticle diffusion model is an external mass transfer explained by the following equation [77–79].

$$q_t = K_{dif} t^{0.5} + C \quad (12)$$

where K_{dif} (mg g^{-1} $min^{-0.5}$) is the intraparticle diffusion rate constant, and C is the intercept. The plot of (q_t) vs. ($t^{0.5}$) shows a multi-linearity relationship, suggesting that the adsorption mechanism is multi-phased (Fig. 8c). The intercept is C, and the rate constant K_{dif} is determined directly from the line's slope (Table 6). Since the resistance to external mass transfer increases as the intercept increases, the value of C provides information about the thickness of the boundary layer. The R^2 values in Table 6 range from 0.688 to 0.990, indicating that the rate-limiting stage for some of the data analyzed is the intra-particle diffusion phase when the R^2 values approach unity. The plots' linearity revealed that intraparticle diffusion inside the particles played a significant role in the chromium adsorption by the adsorbent materials. K_{dif} (intra-particle diffusion rate constants) ranged from 0.02 to 7.69 mg/g $min^{0.5}$. The adsorption of chromium by CTG has low linearity in Fig. 8c, indicating both surface adsorption and intra-particle diffusion are involved in the rate-limiting step. However, there is still no conclusive evidence on which of the two measures was the rate-limiting step. If intraparticle diffusion is the sole rate-limiting stage, the q_t vs. ($t^{0.5}$) plots must move through the origin, which is not the case in this study [77,78]. It can be assumed that during the Cr-CTG reactions, external adsorption with less diffusion inside the particles operated in tandem with an increase in the diffusion fraction

Table 5
For different initial chromium and CTG, the first- and second-order adsorption rate constants, as well as measured and experimental q_e values, were compared.

Parameter			First-order kinetic model			Second-order kinetic model			
CTG (g/L)	Cr(VI) (mg/L)	q_e (exp.) (mg/g)	$K_1 \times 10^3$ (min^{-1})	q_e (calc.) (mg/g)	R^2	$K_2 \times 10^3$ (g/mg min)	q_e (calc.) (mg/g)	h (mg/g min)	R^2
0.5	25	11.633	–2.533	16.081	0.948	5.874	12.207	948.46	0.989
	50	19.082	–2.533	34.770	0.846	2.661	19.930	1279.74	0.998
	75	29.184	–2.073	47.468	0.829	2.769	30.646	2773.07	0.999
	100	31.429	–2.303	65.842	0.859	1.343	31.037	1842.25	0.994
	150	63.776	–0.691	65.645	0.864	8.998	63.516	37452.50	1.000
1.0	25	12.245	–5.297	7.045	0.974	10.978	12.804	1799.76	0.999
	50	18.367	–1.612	16.862	0.933	10.391	18.657	3616.94	0.997
	75	28.027	–1.842	22.872	0.773	12.263	28.571	10010.31	1.000
	100	31.769	–2.303	37.566	0.832	3.023	31.113	3314.63	0.993
	150	56.054	–2.533	41.937	0.854	3.937	56.471	13003.58	0.999
1.5	25	11.173	–19.35	3.834	0.994	20.997	11.534	2793.30	1.000
	50	16.99	–3.224	10.299	0.789	12.623	16.966	4074.42	1.000
	75	25.867	–5.988	18.327	0.779	4.170	25.548	3164.58	0.997
	100	28.265	–1.382	20.893	0.957	11.113	28.563	9066.49	0.999
	150	47.347	–2.994	30.290	0.885	5.8612	47.781	13947.23	1.000
2.0	25	9.469	–11.29	1.261	0.753	50.795	9.653	4733.10	1.000
	50	16.122	–5.527	6.696	0.821	11.772	16.667	3270.13	1.000
	75	22.857	–3.915	10.404	0.474	10.237	23.148	5485.29	0.997
	100	26.327	–2.533	14.093	0.756	14.244	26.738	10183.30	1.000
	150	40.939	–1.612	19.797	0.922	10.959	41.494	18868.68	1.000
2.5	25	7.891	–5.758	0.620	0.765	160.666	7.949	10151.94	1.000
	50	14.66	–6.448	3.682	0.915	19.956	15.038	4512.88	1.000
	75	20.408	–2.994	5.905	0.696	25.636	20.704	10989.02	1.000
	100	24.218	–2.303	10.221	0.968	14.536	24.631	8818.79	0.999
	150	37.313	–2.073	14.581	0.803	8.638	37.736	12300.56	0.999

within the particles as the initial Cr(VI) ions concentration increased.

Another rate equation dependent on adsorption power is the Elovich kinetic equation, commonly expressed as Eq. (13) [80–83].

$$\frac{dq_t}{dt} = \alpha \exp\left(-\beta q_t\right) \tag{13}$$

where α is the initial adsorption rate (mg/g min), and β is desorption constant (g/mg) throughout any trial of adsorption. It is shortened by supposing that $\alpha\beta_t >> t$ and by applying the limit conditions. Eq. (13) can be linearized to Eq. (14).

$$q_t = \frac{1}{\beta}\ln\left(\alpha\beta\right) + \frac{1}{\beta}\ln\left(t\right) \tag{14}$$

A plot of (q_t) against ln(t) should give a linear correlation with a slope of (1/β) and an intercept of 1/β ln(αβ) if Cr(VI) ions adsorption by CTG follows the Elovich model (Fig. 8d). The constants can thus be calculated using the straight-line intercept and slope (Table 6). For most initial Cr(IV) ions concentrations at various adsorbent doses, the R^2 obtained from the Elovich model was significantly higher than those obtained from a pseudo-first-order model.

4. Conclusions

A modified cellulose-TETA-glutraldehyde (CTG) has been established as an efficient adsorbent to extract Cr(VI) ions from its solution after chemical modification of cellulose isolated from rice husk with triethylenetetramine and glutraldehyde. The pH of the adsorption process is essential, and the ideal pH was 1.0. Langmuir, Freundlich, and Temkin isotherms were used to model adsorption studies. For the removal of Cr(VI) ions, an excellent adsorption capacity of 188.68 mg/g was observed. Furthermore, the Freundlich model was found to be the best-fitting model for the adsorption of Cr(VI) ions by CTG in isotherm equilibrium studies. Pseudo-second order kinetics is the most applicable model in adsorbent kinetic studies. The proposed modified adsorbents are efficient, environmentally friendly, and can reduce the massive amount of toxic

Table 6
Using different initial Cr(VI) ions concentrations and CTG doses, the parameters obtained from intraparticle diffusion and the Elovich kinetics model

CTG dose (g/L)	Cr(VI) (mg/L)	Intraparticle diffusion			Elovich		
		K_{dif} (mg/g min$^{0.5}$)	C (mg/g)	R^2	B (g/mg)	α (mg/g min)	R^2
0.5	25	0.5506	5.8364	0.9370	0.59	11.22	0.884
	50	1.3389	6.0944	0.945	0.23	3.42	0.975
	75	1.5668	13.6810	0.919	0.20	13.9944	0.966
	100	2.3565	8.5506	0.950	0.13	4.62	0.963
	150	0.6849	56.9920	0.961	0.45	6.9×10^{10}	0.983
1.0	25	0.3972	8.1268	0.987	0.795	163.703	0.974
	50	0.3963	13.8570	0.901	0.787	13,671.2	0.911
	75	0.5441	22.7350	0.871	0.557	104,408	0.933
	100	1.2889	17.6580	0.920	0.239	54.909	0.952
	150	1.2132	43.460	0.939	0.261	64,909.6	0.924
1.5	25	0.2807	8.4463	0.938	1.095	1,810.82	0.976
	50	0.4960	12.3440	0.911	0.619	641.494	0.950
	75	1.1171	14.790	0.854	0.277	42.5244	0.874
	100	0.4146	23.760	0.949	0.763	2×10^7	0.932
	150	1.0504	37.2110	0.929	0.293	35,366.3	0.965
2.0	25	0.1599	8.0029	0.812	1.879	327,532	0.884
	50	0.4897	11.2810	0.866	0.617	315.424	0.931
	75	0.5720	16.8770	0.681	0.514	1,977.5	0.774
	100	0.4317	22.0230	0.854	0.702	1,361,627	0.914
	150	0.5058	35.7910	0.977	0.618	1.3×10^9	0.982
2.5	25	0.0492	7.4318	0.854	6.158	2.3×10^{18}	0.914
	50	0.2753	11.9320	0.957	1.132	126,219	0.969
	75	0.2725	17.8080	0.787	1.107	6×10^7	0.850
	100	0.2995	20.9830	0.941	1.079	1.4×10^9	0.886
	150	0.4251	32.3450	0.792	0.772	2×10^{10}	0.723

chromium ions released into the aquatic environment due to waste discharges. It was revealed that an adsorbent developed from modified rice husk cellulose (CTG) was effective in removing Cr(VI) ions from water.

Acknowledgements

The authors would like to thanks financial support from Science and Technological Development Fund (STDF) of Egypt (Project No. CB-4874, CB-22816 and IG-34795).

Conflict of interests

The authors declare that they have no known conflict of interests or personal relationships that could have appeared to influence the work reported in this paper.

References

[1] C. Zinge, B. Kandasubramanian, Nanocellulose based biodegradable polymers, Eur. Polym. J., 133 (2020) 109758, doi: 10.1016/j.eurpolymj.2020.109758.
[2] E.J. Cho, L.T.P. Trinh, Y. Song, Y.G. Lee, H.-J. Bae, Bioconversion of biomass waste into high value chemicals, Bioresour. Technol., 298 (2020) 122386, doi: 10.1016/j.biortech.2019.122386.
[3] K.F. Mahmoud, S.C. Alfaro, O. Favez, M.M. Abdel Wahab, J. Sciare, Origin of black carbon concentration peaks in Cairo (Egypt), Atmos. Res., 89 (2008) 161–169.
[4] A. El Nemr, Non-Conventional Textile Waste Water Treatment, Nova Science Publishers, Inc., Hauppauge New York, 2012. [Hard Cover ISBN: 978-1-62100-079-2, e-book ISBN: 978-1-62100-228-4] 267 pages.
[5] A. El Nemr, A. Khaled, O. Abdelwahab, A. El-Sikaily, Treatment of wastewater containing toxic chromium using new activated carbon developed from date palm seed, J. Hazard. Mater., 152 (2008) 263–275.
[6] A. El Nemr, A. El-Sikaily, A. Khaled, Modeling of adsorption isotherms of Methylene Blue onto rice husk activated carbon, Egypt. J. Aquat. Res., 36 (2010) 403–425.
[7] A. El Nemr, A. El-Sikaily, A. Khaled, O. Abdelwahab, Removal of toxic chromium from aqueous solution, wastewater and saline water by marine red alga *Pterocladia capillacea* and its activated carbon, Arabian J. Chem., 8 (2015) 105–117.
[8] H. Guo, S. Zhang, Z. Kou, S. Zhaib, W. Ma, Y. Yang, Removal of cadmium(II) from aqueous solutions by chemically modified maize straw, Carbohydr. Polym., 115 (2015) 177–185.
[9] A. Eleryan, A. El Nemr, M. Mashaly, A. Khaled, 6-Triethylenetetramine 6-deoxycellulose grafted with crotonaldehyde as adsorbent for Cr^{6+} removal from wastewater, Int. J. Sci. Eng. Res., 10 (2019) 1199–1211.
[10] A. Eleryan, A. El Nemr, M.M. Alghamdi, A.A. El-Zahhar, A.M. Idris, Feasible and eco-friendly removal of hexavalent chromium toxicant from aqueous solutions using chemically

modified sugarcane bagasse cellulose, Toxin Rev., 40 (2021) 835–846.
[11] M.K.M. Haafiz, A. Hassan, Z. Zakaria, I.M. Inuwa, Isolation and characterization of cellulose nanowhiskers from oilpalm biomass microcrystalline cellulose, Carbohydr. Polym., 103 (2014) 119–125.
[12] C. Zhong, C. Wang, F. Huang, H. Jia, P. Wei, Wheat straw cellulose dissolution and isolation by tetra-*n*-butylammonium hydroxide, Carbohydr. Polym., 94 (2013) 38–45.
[13] H.K. Shin, J.P. Jeun, H.B. Kim, P.H. Kang, Isolation of cellulose fibers from kenaf using electron beam, Radiat. Phys. Chem., 81 (2012) 936–940.
[14] C. Mu, M. Jiang, J. Zhu, M. Zhao, S. Zhu, Z. Zhou, Isolation of cellulose from steam-exploded rice straw with aniline catalyzing dimethyl formamide aqueous solution, Renewable Energy, 63 (2014) 324–329.
[15] M. Jiang, M. Zhao, Z. Zhou, T. Huang, X. Chen, Y. Wang, Isolation of cellulose with ionic liquid from steam exploded rice straw, Ind. Crops Prod., 33 (2011) 734–738.
[16] I. Bicu, F. Mustata, Optimization of isolation of cellulose from orange peel using sodium hydroxide and chelating agents, Carbohydr. Polym., 98 (2013) 341–348.
[17] M.L. Hassan, J. Brasc, E.A. Hassan, C. Silard, E. Mauret, Enzyme-assisted isolation of micro fibrillated cellulose from date palm fruit stalks, Ind. Crops Prod., 55 (2014) 102–108.
[18] S.M.A.S. Keshk, M.A. Haija, A new method for producing microcrystalline cellulose from *Gluconacetobacter xylinus* and kenaf, Carbohydr. Polym., 84 (2011) 1301–1305.
[19] C.S. Patil, D.B. Gunjal, V.M. Naik, N.S. Harale, S.D. Jagadale, A.N. Kadam, P.S. Patil, G.B. Kolekar, A.H. Gore, Waste tea residue as a low cost adsorbent for removal of hydralazine hydrochloride pharmaceutical pollutant from aqueous media: An environmental remediation, J. Cleaner Prod., 206 (2019) 407–418.
[20] M. Corral-Bobadilla, A. González-Marcos, F. Alba-Elías, E.D. de Santo Domingo, Valorization of bio-waste for the removal of aluminum from industrial wastewater, J. Cleaner Prod., 264 (2021) 121608, doi: 10.1016/j.jclepro.2020.121608.
[21] A. El Nemr, M.N.M. Ismail, E.S.H. El Ashry, H. Abdel Hamid, Novel simple modification of chitosan as adsorptive agent for removal of Cr^{6+} from aqueous solution, Egypt. J. Chem., 63 (2020) 1219–1240.
[22] T.M. Eldeeb, A. El Nemr, M.H. Khedr, S.I. El-Dek, N.G. Imam, Novel, Three-dimensionoal, chitosan-carbon nanotube–PVA nanocomposite hydrogel for removal of Cr^{6+} from water, Desal. Water Treat., 184 (2020) 163–177.
[23] A. Guleria, G. Kumari, E.C. Lima, Cellulose-g-poly-(acrylamide-co-acrylic acid) polymeric bioadsorbent for the removal of toxic inorganic pollutants from wastewaters, Carbohydr. Polym., 228 (2020) 115396, doi: 10.1016/j.carbpol.2019.115396.
[24] A. El Nemr, S. Ragab, Acetylation of Cotton-Giza 86 cellulose using $MnCl_2$ as a new catalyst and its application to machine oil removal, Environ. Process., 5 (2018) 895–905.
[25] J.O. Zoppe, P.A. Larsson, O. Cusola, Chapter 2 – Surface Modification of Nanocellulosics and Functionalities, Lignocellulosics, Renewable Feedstock for (Tailored) Funct. Mater. Nanotechnol., 2020, pp. 17–63. Available at: https://doi.org/10.1016/B978-0-12-804077-5.00003-8
[26] B. Hashemi, P. Zohrabi, M. Shamsipur, Recent developments and applications of different sorbents for SPE and SPME from biological samples, Talanta, 187 (2018) 337–347.
[27] A. El Nemr, A.A. Moneer, A. Khaled, A. El-Sikaily, Levels, distribution and risk assessment of organochlorines in surficial sediments of the Red Sea coast, Egypt, Environ. Monit. Assess., 185 (2013) 4835–4853.
[28] A. El Nemr, A.A. Moneer, S. Ragab, A. El Sikaily, Distribution and sources of *n*-alkanes and polycyclic aromatic hydrocarbons in Shellfish of the Egyptian Red Sea coast, Egypt. J. Aquat. Res., 42 (2016) 121–131.
[29] A. El Nemr, G.F. El-Said, A. Khaled, S. Ragab, Distribution and ecological risk assessment of some heavy metals in coastal surface sediments along the Red Sea, Egypt. Int. J. Sediment. Res., 31 (2016) 164–172.
[30] D.M.S. Salem, A. Khaled, A. El Nemr, Assessment of pesticides and polychlorinated biphenyls (PCBs) in sediments of the Egyptian Mediterranean Coast, Egypt. J. Aquat. Res., 39 (2013) 141–152.
[31] D.M.S.A. Salem, A. El Sikaily, A. El Nemr, Organocholorines and their risk in marine shellfish collected from the Mediterranean coast, Egypt, Egypt. J. Aquat. Res., 40 (2014) 93–101.
[32] D.M.S.A. Salem, A. Khaled, A. El Nemr, A. El-Sikaily, Comprehensive risk assessment of heavy metals in surface sediments along the Egyptian Red Sea coast, Egypt. J. Aquat. Res., 40 (2014) 349–362.
[33] D.M.S.A. Salem, F.A.-E.M. Morsy, A. El Nemr, A. El-Sikaily, A. Khaled, The monitoring and risk assessment of aliphatic and aromatic hydrocarbons (PAHs) in sediments of the Red Sea, Egypt, Egypt. J. Aquat. Res., 40 (2014) 333–348.
[34] S. Ragab, A. El Sikaily, A. El Nemr, Concentrations and sources of pesticides and PCBs in surficial sediments of the Red Sea Coast, Egypt, Egypt. J. Aquat. Res., 42 (2016) 365–374.
[35] A.M. Idris, T.O. Said, E.I. Brima, T. Sahlabji, M.M. Alghamdi, A.A. El-Zahhar, M. Arshad, A.M. El Nemr, Assessment of contents of selected heavy metals in street dust from Khamees-Mushait city, Saudi Arabia, using multivariate statistical analysis, GIS mapping, geochemical indices and health risk, Fresenius Environ. Bull., 28 (2019) 6059–6069.
[36] H.F.M. Asiri, A.M. Idris, T.O. Said, T. Sahlabji, M.M. Alghamdi, A.A. El-Zahhar, E.-A. Nemr, Monitoring and health risk assessment of some pesticides and organic pollutants in fruit and vegetables consumed in Asir Region, Saudi Arabia, Fresenius Environ. Bull., 29 (2020) 615–625.
[37] A. Kadama, R. Govind, B. Nairb, S.J. Dhoble, Insights into the extraction of mercury from fluorescent lamps: a review, J. Environ. Chem. Eng., 7 (2019) 103279, doi: 10.1016/j.jece.2019.103279.
[38] A.R.K. Gollakota, S. Gautam, C.-M. Shu, Inconsistencies of e-waste management in developing nations – facts and plausible solutions, J. Environ. Manage., 261 (2020) 110234, doi: 10.1016/j.jenvman.2020.110234.
[39] E. Serag, A. El Nemr, A. El-Maghraby, Synthesis of highly effective novel graphene oxide-polyethylene glycol-polyvinyl alcohol nanocomposite hydrogel for copper removal, J. Water Environ. Nanotechnol., 2 (2017) 223–234.
[40] E. Serag, A. El Nemr, F.F. Abdel Hamid, S.A. Fathy, A. El-Maghraby, A novel three dimensional carbon nanotube-polyethylene glycol – polyvinyl alcohol nanocomposite for Cu(II) removal from water, Egypt. J. Aquat. Biol. Fisher., 22 (2018) 103–118.
[41] S. Meseldzija, J. Petrovic, A. Onjia, T. Volkov-Husovic, A. Nesic, N. Vukelic, Utilization of agro-industrial waste for removal of copper ions from aqueous solutions and mining-wastewater, J. Ind. Eng. Chem., 75 (2019) 246–252.
[42] M.A. El-Nemr, I.M.A. Ismail, N.M. Abdelmonem, S. Ragab, A. El Nemr, Ozone and ammonium hydroxide modification of biochar prepared from *Pisum sativum* peels improves the adsorption of copper(II) from an aqueous medium, Environ. Proc., 7 (2020) 973–1007.
[43] M.A. El-Nemr, I.M.A. Ismail, N.M. Abdelmonem, A. El Nemr, S. Ragab, Amination of biochar derived from Watermelon peel by triethylenetetramine and ammonium hydroxide for toxic chromium removal enhancement, Chin. J. Chem. Eng., 36 (2021) 199–222.
[44] M.A. El-Nemr, I.M.A. Ismail, N.M. Abdelmonem, S. Ragab, A. El Nemr, The efficient removal of the hazardous Azo Dye Acid Orange 7 from water using modified biochar from Pea peels, Desal. Water Treat., 203 (2020) 327–355.
[45] M.A. El-Nemr, I.M.A. Ismail, N.M. Abdelmonem, S. Ragab, A. El Nemr, Removal of Acid Yellow 11 Dye using novel modified biochar derived from Watermelon Peels, Desal. Water Treat., 203 (2020) 403–431.
[46] T. Sahlabji, A. El Nemr, S. Ragab, M.M. Alghamdi, A.A. El-Zahhar, A.M. Idris, T.O. Said, High surface area microporous activated carbon from *Pisum sativum* peels for hexavalent chromium removal from aquatic environment, Toxin Rev., (2021) (In Press), doi: 10.1080/15569543.2021.1908361.

[47] D.W. O'Connell, C. Birkinshaw, T.F. O'Dwyer, Heavy metal adsorbents prepared from the modification of cellulose: a review, Bioresour. Technol., 99 (2008) 6709–6724.
[48] D. Lu, Q. Cao, X. Li, X. Cao, F. Luo, W. Shao, Kinetics and equilibrium of Cu(II) adsorption onto chemically modified orange peel cellulose biosorbents, Hydrometallurgy, 95 (2009) 145–152.
[49] L. Zhou, Y. Duan, X. Xu, Facile preparation of amine-rich polyamidoamine (PAMAM) gel for highly efficient removal of Cr(VI) ions, Colloids Surf., A, 579 (2019) 123685, doi: 10.1016/j.colsurfa.2019.123685.
[50] J. Tan, Y. Song, X. Huang, L. Zhou, Facile functionalization of natural peach gum polysaccharide with multiple amine groups for highly efficient removal of toxic hexavalent chromium (Cr(VI)) ions from water, ACS Omega, 3 (2018) 17309–17318.
[51] O. Abdelwahab, A. El Sikaily, A. Khaled, A. El Nemr, Mass transfer processes of chromium(VI) adsorption onto Guava seeds, Chem. Ecol., 23 (2007) 73–85.
[52] A. El Nemr, A. El Sikaily, A. Khaled, O. Abdelwahab, Removal of toxic chromium(VI) from aqueous solution by activated carbon using *Casuarina Equisetifolia*, Chem. Ecol., 23 (2007) 119–129.
[53] WHO, Originally Published in Guidelines for Drinking-Water Quality, 2nd ed., Vol. 2, Health Criteria and Other Supporting Information, World Health Organization, Geneva, 1996.
[54] A. El Nemr, Potential of pomegranate husk carbon for Cr(VI) removal from wastewater: kinetic and isotherm studies, J. Hazard. Mater., 161 (2009) 132–141.
[55] J.C. Almeida, C.E.D. Cardoso, D.S. Tavares, R. Freitas, T. Trindade, C. Vale, E. Pereira, Chromium removal from contaminated waters using nanomaterials. A review, Trends Anal. Chem., 118 (2019) 277–291.
[56] S.A. Kedzior, J.O. Zoppe, R.M. Berry, E.D. Cranston, Recent advances and an industrial perspective of cellulose nanocrystal functionalization through polymer grafting, Curr. Opin. Solid State Mater. Sci., 23 (2019) 74–91.
[57] H. Gao, L.-L. Fu, M.-L. Cai, W. Chen, Z.-W. Bai, Preparation of 6-amino-6-deoxy cellulose and its derivatives used as chiral separation materials, Carbohydr. Polym., 259 (2021) 117756, doi: 10.1016/j.carbpol.2021.117756.
[58] W. Bessa, A.F. Tarchoun, D. Trache, M. Derradji, Preparation of amino-functionalized microcrystalline cellulose from *Arundo Donax* L. and its effect on the curing behavior of bisphenol A–based benzoxazine, Thermochim. Acta, 698 (2021) 178882, doi: 10.1016/j.tca.2021.178882.
[59] M. Shokri, S. Moradi, S. Amini, M. Shahlaei, F. Seidi, S. Saedi, A novel amino cellulose derivative using ATRP method: preparation, characterization, and investigation of its antibacterial activity, Bioorg. Chem., 106 (2021) 104355, doi: 10.1016/j.bioorg.2020.104355.
[60] Y. Dong, Y. Lai, X. Wang, M. Gao, F. Xue, X.F. Chen, Y. Ma, Y. Wei, Design and synthesis of amine-functionalized cellulose with multiple binding sites and their application in C-C bond forming reactions, Int. J. Biol. Macromol., 130 (2019) 778–785.
[61] S. Ragab, A. El Nemr, Nanofiber cellulose di- and tri-acetate using ferric chloride as a catalyst promoting highly efficient synthesis under microwave irradiation, J. Macromol. Sci. Part A Pure Appl. Chem., 55 (2018) 124–134.
[62] S. Ragab, A. El Nemr, Zirconyl chloride as a novel and efficient green Lewis acid catalyst for direct acetylation of cotton cellulose in the presence and absence of solvent, J. Polym. Res., 26 (2019) 156, doi: 10.1007/s10965-019-1816.
[63] A. El Nemr, S. Ragab, A. El Sikaily, Rapid synthesis of cellulose triacetate from cotton cellulose and its effect on specific surface area and particle size distribution, Iran Polym. J., 26 (2017) 261–272.
[64] T.A. Maxcy, G. Paul Willhite, D.W. Green, K. Bowman-James, A kinetic study of the reduction of chromium(VI) to chromium (III)/by thiourea, J. Pet. Sci. Eng., 19 (1998) 253–263.
[65] E. Malkoc, Y. Nuhoglu, The removal of chromium(VI) from synthetic wastewater by *Ulothrix zonata*, Fresenius Environ. Bull., 12 (2001) 361–376.
[66] I. Langmuir, The constitution and fundamental properties of solids and liquids, J. Am. Chem. Soc., 38 (1916) 2221–2295.
[67] D.G. Kinniburgh, General purpose adsorption isotherms, Environ. Sci. Technol., 20 (1986) 895–904.
[68] E. Longhinotti, F. Pozza, L. Furlan, M.D.N.D. Sanchez, M. Klug, M.C.M. Laranjeira, V.T. Favere, Adsorption of anionic dyes on the biopolymer chitin, J. Braz. Chem. Soc., 9 (1998) 435–440.
[69] H.M.F. Freundlich, Uber die adsorption in lo sungen, Zeitschrift fur Physikalische Chemie (Leipzig), 57A (1906) 385–470.
[70] C. Aharoni, M. Ungarish, Kinetics of activated chemisorption. Part 2. Theoretical models, J. Chem. Soc. Faraday Trans., 73 (1977) 456–464.
[71] C. Aharoni, D.L. Sparks, Kinetics of Soil Chemical Reactions-A Theoretical Treatment, D.L. Sparks, D.L. Suarez, Eds., Rate of Soil Chem. Process., Soil Sci. Soc. Am., Madison, WI, 1991, pp. 1–18.
[72] X.S. Wang, Y. Qin, Equilibrium sorption isotherms for of Cu^{2+} on rice bran, Process Biochem., 40 (2005) 677–680.
[73] C.I. Pearce, J.R. Lioyd, J.T. Guthrie, The removal of color from textile wastewater using whole bacterial cells: a review, Dyes Pigm., 58 (2003) 179–196.
[74] G. Akkaya, A. Ozer, Adsorption of acid red 274 (AR 274) on *Dicranella varia*: determination of equilibrium and kinetic model parameters, Process Biochem., 40 (2005) 3559–3568.
[75] S. Lagergren, Zur theorie der sogenannten adsorption geloster stoffe, Kungliga Svenska Vetenskapsakademiens, Handlingar, 24 (1898) 1–39.
[76] Y.S. Ho, G. McKay, D.A.J. Wase, C.F. Foster, Study of the sorption of divalent metal ions on to peat, Adsorpt. Sci. Technol., 18 (2000) 639–650.
[77] W.J. Weber, J.C. Morris, Kinetics of adsorption on carbon from solution, J. Sanit. Eng. Div. Am. Soc. Civ. Eng., 89 (1963) 31–60.
[78] K. Srinivasan, N. Balasubramanian, T.V. Ramakrishan, Studies on chromium removal by rice husk carbon, Ind. J. Environ. Health., 30 (1988) 376–387.
[79] M.N.M. Ismael, A. El Nemr, E.S.H. El Ashry, H. Abdel Hamid, Removal of hexavalent chromium by cross-linking chitosan and *N,N*›-methylene bis-acrylamide, Environ. Process., 7 (2020) 911–930.
[80] J. Zeldowitsch, Uber den mechanismus der katalytischen oxidation von CO an MnO_2, Acta Physicochim, URSS, 1 (1934) 364–449.
[81] S.H. Chien, W.R. Clayton, Application of Elovich equation to the kinetics of phosphate release and sorption on soils, Soil Sci. Soc. Am. J., 44 (1980) 265–268.
[82] D.L. Sparks, Kinetics of Reaction in Pure and Mixed Systems, in: Soil Physical Chemistry, CRC Press, Boca Raton, 1986.
[83] A. El Nemr, Pomegranate husk as an adsorbent in the removal of toxic chromium from wastewater, Chem. Ecol., 23 (2007) 409–425.